Chapter 2

Compact discretization of 3D generalized convection-diffusion equation with variable coefficients on nonuniform grids

2.1 Introduction

In this chapter, we lay our emphasis on the steady generalized CDE in three dimensions. For the transport variable $\phi(x, y, z)$ over a cuboidal region $\Omega \subset \mathbb{R}^3$, the CDE (1.4) in steady form is written as

$$-\nabla \cdot (\boldsymbol{D}\nabla\phi) + \nabla \cdot (\boldsymbol{C}\phi) = s \tag{2.1}$$

with boundary condition

$$\phi = \phi^b \ \text{ on } \ \partial\Omega. \tag{2.2}$$

We work with a fully populated positive definite diffusion matrix $\boldsymbol{D}$ which along with $\boldsymbol{C}$ in three dimensions (3D) is given by

$$\boldsymbol{D} = \begin{bmatrix} a_1 & -d_1/2 & -d_3/2 \\ -d_1/2 & a_2 & -d_2/2 \\ -d_3/2 & -d_2/2 & a_3 \end{bmatrix}, \quad \boldsymbol{C} = \begin{bmatrix} c_1 \\ c_2 \\ c_3 \end{bmatrix}.$$

As mentioned in the previous chapter for the unknown function $\phi(x, y, z)$ in equation (1.4), we assume the variable coefficient functions $a_i(x, y, z)$, $d_i(x, y, z)$, $c_i(x, y, z)$, $i \in \{1, 2, 3\}$ and the forcing function $s(x, y, z, \phi)$ to have sufficient smoothness in Ω.

Using mathematical simplification, we can write the nonconservative form of equation (1.4) as

$$\big(-a_1\partial_{xx} - a_2\partial_{yy} - a_3\partial_{zz} + d_1\partial_{xy} + d_2\partial_{yz} + d_3\partial_{zx} + e_1\partial_x + e_2\partial_y + e_3\partial_z\big)\phi = f \quad (2.3)$$

where

$$e_1 = -\frac{\partial a_1}{\partial x} + \frac{1}{2}\left(\frac{\partial d_1}{\partial y} + \frac{\partial d_1}{\partial z}\right) + c_1,$$

$$e_2 = -\frac{\partial a_2}{\partial y} + \frac{1}{2}\left(\frac{\partial d_2}{\partial z} + \frac{\partial d_2}{\partial x}\right) + c_2,$$

$$e_3 = -\frac{\partial a_3}{\partial z} + \frac{1}{2}\left(\frac{\partial d_3}{\partial x} + \frac{\partial d_3}{\partial y}\right) + c_3$$

and

$$f = s - \left(\frac{\partial c_1}{\partial x} + \frac{\partial c_2}{\partial y} + \frac{\partial c_3}{\partial z}\right)\phi.$$

The importance and relevance of CDE has been thoroughly discussed in Chapter 1. It is well known that CDE finds applications in a diverse range of processes as it correctly models convection and diffusion of various physical quantities. CDE is well established in areas as diverse as biology, environmental science, financial mathematics, and even sociology, in addition to chemical and physical systems. The underlying system in many of these cases is three dimensional. However, due to the prohibitive cost of computing, attempts to simulate the solution of CDE are frequently limited to one dimension (1D) or two dimensions (2D). Another simplification assumption often imposed on CDE is that the diffusion matrix instead of being fully populated is considered to be an identity matrix. It is well documented in the literature that the generalized CDE with mixed derivatives plays a significant role in domains like mathematical biology [65] and financial mathematics [37, 64, 66]. Mixed derivatives signify correlations between the underlying processes. Further, while applying coordinate transforms to CDE on nonrectangular domains one must deal with the mixed-derivative terms in the transformed equation [116, 150]. However, the presence of second-order mixed-derivative terms introduces new challenges towards the solvability of the generalized CDE.

The FD method has traditionally been recognized as the most promising numeri-

cal methodology for solving CDE and is widely employed [2, 3, 33, 57, 104, 107, 108]. The enduring popularity of these methods can be gauged from continuous efforts in the literature to develop even more efficient compact schemes [130, 131, 156, 160]. Discretization strategies are frequently established by analyzing one dimensional (1D) and two dimensional (2D) CDE, and their derivation to 3D generalized CDE may be involved. The pioneering work on 3D generalized CDE was carried out by Ananthakrisnaiah *et al.* [3] by generalizing the strategy developed in [2]. The authors created a fourth-order accurate FD method on uniform grids employing 27 grid points in the presence of the cross-derivative terms in this study. That was the first time a compact system of 27 points for 3D CDE was reported. This benchmark work inspired several breakthroughs in FD discretizations especially for the 3D Poisson equation [55, 108, 149, 152, 179]. In their work, Mohanty and Jain [108] developed a fourth-order compact scheme for solving system of nonlinear elliptic PDE with variable coefficients. The authors put their system through its paces on a variety of problems, including 3D Poisson equation and steady-state viscous incompressible N-S equations in polar coordinates. The duo successfully yielded oscillation-free and accurate solutions for large values of Re even in the vicinity of singularity. In the recent two decades, this has been followed by further advancement of 3D compact techniques for nonlinear and quasi-linear elliptic PDE [104, 105, 106]. In 1998, Zhang [179] made an effort to investigate generalized dominion for problems and introduced an explicit fourth-order FD compact scheme for 3D CDE with variable convection coefficients. For low and moderate Re values ($0 \leq Re \leq 10^3$), the scheme returned stable and high-accuracy solutions. The computed accuracy was reported to reduce to second-order for large Re ($\geq 10^4$), yet carrying higher accuracy than the first-order upwind difference scheme then existed. Zhang [180], in 1998, further came up with a fourth-order compact FD scheme with the multigrid algorithm to solve the 3D Poisson equation. In the subsequent years, Ge [49] and Ge *et al.* [51] used the similar approach to tackle 3D Poisson equation. Earlier in this century, FD schemes for 3D linear elliptic PDE were also put forth [28, 29]. High accuracy solution of 3D CDE using multigrid strategy was also reported in the work of Gupta and Zhang [56] and Wang and Zhang [166]. Recent years have witnessed several

developments of FD based compact schemes for the 3D CDE. Among them, special attention should be paid to the work of Zhang *et al.* [182], Karaa [79], Ma and Ge [101], Ge *et al.* [50], Mohamed *et al.* [103] and Ma and Ge [100]. However, as previously stated, CDE in the presence of mixed derivative terms has not yet been utterly explored. Here, it is important to cite a few recent works on 2D CDE with mixed derivatives [42, 80, 94, 131]. But similar studies on 3D CDE with mixed derivative [3, 81, 104] has gained lesser attention. Fournié and Karaa [42] in 2006 solved elliptic partial differential equation (PDE) in the presence of mixed derivatives and constant coefficients. The authors used the PDE itself as an auxiliary relation to derive a 9 point fourth-order compact finite difference scheme. The scheme was limited to the unit diffusion coefficient. In another work, by developing a fourth-order compact FD scheme using polynomial approximation, Karaa [80] solved 2D parabolic and elliptic problems with mixed derivatives and variable coefficients, yet again with the same restrictions on diffusion coefficients and mixed derivative coefficients as in [42]. Later on, the idea was expanded upon by Karaa and Othman [81] for time-dependent 3D parabolic problems in the presence of mixed derivatives. Along with FD compact systems, researchers have developed a number of other notable approaches to deal with steady CDE in 3D, both with [4, 97, 124, 141] and without [165] mixed derivatives, throughout the years.

It is observed that at times uniform grid-based systems efficiently generate highly accurate, stable numerical solutions but fall short of exhibiting the advantages of nonuniform grids. This is especially true in the higher gradient regions of the flow variables where it is essential to resolve small scales. One such conundrum appears when CDE becomes convection-dominated or singularly perturbed. Solutions of singularly perturbed CDE generally consist of some boundary layers and/or inner layers. Only by setting up very finer meshes can these high gradient regions be resolved, which escalates the computational cost of any discretization on uniform grids and reduces the precision of the solution. One of the more effective methods of efficient computation for these kinds of problems is to spread out the grids in regions of low gradient and cluster them in regions with higher gradient. Not only it could resolve smaller scales accurately, substantial reduction in compu-

tation time could also be seen. Hence, for many flow configurations it is recommended to use nonuniform meshes. One way to circumvent the use of computation on the nonuniform grid is to use a suitable transformation from the physical domain to the numerical domain to capture the boundary layers efficiently. This approach, followed elsewhere [131, 181], brings in its own set of advantages and disadvantages and will not be adopted here. Furthermore, strategies developed on nonuniform grids report back higher accuracy with the adoption of uniform spacing. Thus, in cases where schemes could be developed on nonuniform grids, they tend to be the sought after abstraction. Although, over the years, for 2D CDE a plethora of transformation-free compact schemes are developed on nonuniform grids [16, 30, 46, 47, 77, 78, 86, 120, 127, 150, 156, 158, 159, 160] but sufficient attention has not been provided towards the development of compact discretization for 3D CDE in the nonuniform grid. Here, it is important to mention that recently Ge *et al.* [51] proposed the first transformation-free higher order compact scheme and multigrid method to solve the 3D Poisson equation on nonuniform grids. The scheme reported accuracy of order four under uniform grid setting and third to fourth-order accuracy on nonuniform grids. To the best of the authors knowledge, no compact schemes could be found in the literature which approximates 3D CDE with cross-derivative terms on nonuniform grids.

Having recognized the challenges and potential, the main motivation of this chapter is to develop compact discretization of the 3D generalized CDE (2.3) on nonuniform grids without coordinate transformation. The present scheme is employed to eight diverse numerical test cases with varied complexities and the results are compared to those available in the literature.

2.2 Numerical scheme development

We carry out the discretization process on a nonuniform 3D grid. Thus, we first consider a cuboidal domain $\Omega = [a_x, b_x] \times [a_y, b_y] \times [a_z, b_z]$ in $\mathbb{R}^3$. We take refinements

for the intervals $[a_x, b_x]$, $[a_y, b_y]$ and $[a_z, b_z]$ as

$$a_x = x_1 < x_2 < x_3 < \cdots < x_{n_x} = b_x,$$
$$a_y = y_1 < y_2 < y_3 < \cdots < y_{n_y} = b_y,$$
$$a_z = z_1 < z_2 < z_3 < \cdots < z_{n_z} = b_z,$$

where x_i's, $i \in \{1, 2, 3, \ldots, n_x\}$, y_j's, $j \in \{1, 2, 3, \ldots, n_y\}$ and z_k's, $k \in \{1, 2, 3, \ldots, n_z\}$ need not be equally spaced. A grid generated in this fashion can be witnessed in Fig. 2.1. Along x-, y- and z-directions the mesh sizes are given by

$$h_{x_i} = x_{i+1} - x_i, \quad i \in \{1, 2, 3, \ldots, n_x - 1\},$$
$$h_{y_j} = y_{j+1} - y_j, \quad j \in \{1, 2, 3, \ldots, n_y - 1\},$$
$$h_{z_k} = z_{k+1} - z_k, \quad k \in \{1, 2, 3, \ldots, n_z - 1\}.$$

These grid spacing varies with node and to cutback the complications of the scheme furthermore, we define

$$\alpha_{x_i} = h_{x_{i+1}}/h_{x_i}, \quad i \in \{1, 2, 3, \ldots, n_x - 2\},$$
$$\alpha_{y_j} = h_{y_{j+1}}/h_{y_j}, \quad j \in \{1, 2, 3, \ldots, n_y - 2\},$$
$$\alpha_{z_k} = h_{z_{k+1}}/h_{z_k}, \quad k \in \{1, 2, 3, \ldots, n_z - 2\}.$$

Although α_{x_i}, $i \in \{1, 2, 3, \ldots, n_x - 2\}$, α_{y_j}, $j \in \{1, 2, 3, \ldots, n_y - 2\}$ and α_{z_k}, $k \in \{1, 2, 3, \ldots, n_z - 2\}$ are arrays of real numbers and their values vary with change in grid points, we shall drop the suffixes i, j and k from α_{x_i}, α_{y_j} and α_{z_k} for brevity and shall refer them as α_x, α_y and α_z respectively in the subsequent sections of the chapter. It should also be mentioned that whenever the values α_x, α_y and α_z become unity the mesh turns to be a uniform one.

First and second-order finite difference operators in the x-direction, δ_x and δ_x^2, are defined as

$$\delta_x \phi_{i,j,k} = \frac{1}{h_{x_i} + h_{x_{i-1}}} \left(\phi_{i+1,j,k} - \phi_{i-1,j,k}\right) \tag{2.4}$$

and

$$\delta_x^2 \phi_{i,j,k} = \frac{2}{h_{x_i} + h_{x_{i-1}}} \left[\frac{\phi_{i+1,j,k}}{h_{x_i}} + \frac{\phi_{i-1,j,k}}{h_{x_{i-1}}} - \left(\frac{1}{h_{x_i}} + \frac{1}{h_{x_{i-1}}}\right) \phi_{i,j,k}\right] \tag{2.5}$$

respectively, where $\phi_{i,j,k} = \phi(x_i, y_j, z_k)$. For the sufficiently smooth transport variable $\phi(x, y, z)$, the first and second-order partial derivatives, $\partial_x \phi$ and $\partial_{xx} \phi$ respec-

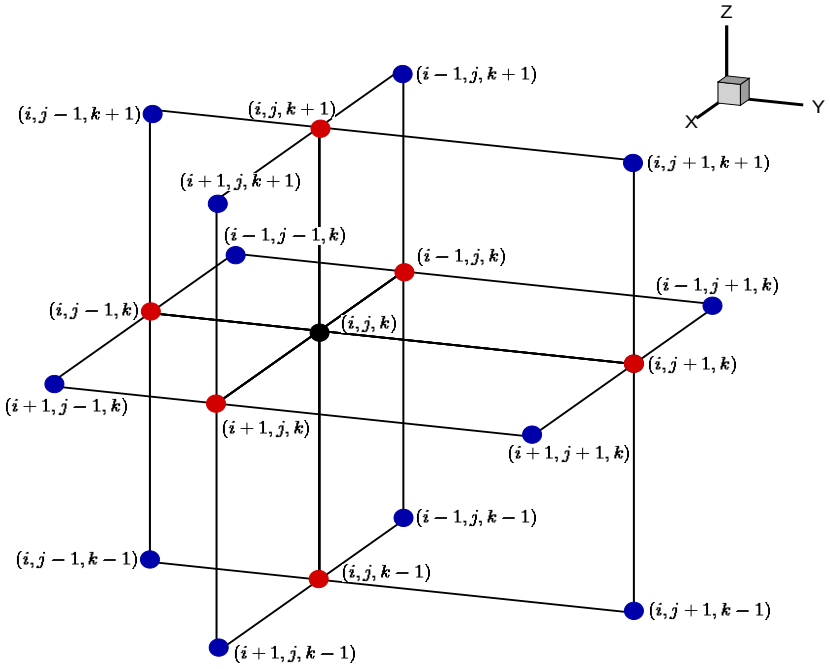

Fig. 2.1: The nineteen point compact nonuniform computational stencil used for discretization.

tively, along the x-direction, at a point (x_i, y_j, z_k) lying inside the reference cube can be approximated using the Taylor series expansion as

$$\begin{aligned}\partial_x\phi_{i,j,k} = \delta_x\phi_{i,j,k} - \frac{1}{2}\left(h_{x_i} - h_{x_{i-1}}\right)\partial_{xx}\phi_{i,j,k} - \frac{1}{6}\left(\frac{h_{x_i}^3 + h_{x_{i-1}}^3}{h_{x_i} + h_{x_{i-1}}}\right)\partial_{xxx}\phi_{i,j,k} \\ - \frac{1}{24}\left(\frac{h_{x_i}^4 - h_{x_{i-1}}^4}{h_{x_i} + h_{x_{i-1}}}\right)\partial_{xxxx}\phi_{i,j,k} + \mathcal{O}\left(\frac{h_{x_i}^5 + h_{x_{i-1}}^5}{h_{x_i} + h_{x_{i-1}}}\right)\end{aligned} \tag{2.6}$$

and

$$\begin{aligned}\partial_{xx}\phi_{i,j,k} = \delta_x^2\phi_{i,j,k} - \frac{1}{3}\left(h_{x_i} - h_{x_{i-1}}\right)\partial_{xxx}\phi_{i,j,k} - \frac{1}{12}\left(\frac{h_{x_i}^3 + h_{x_{i-1}}^3}{h_{x_i} + h_{x_{i-1}}}\right)\partial_{xxxx}\phi_{i,j,k} \\ - \frac{1}{60}\left(\frac{h_{x_i}^4 - h_{x_{i-1}}^4}{h_{x_i} + h_{x_{i-1}}}\right)\partial_{xxxxx}\phi_{i,j,k} + \mathcal{O}\left(\frac{h_{x_i}^5 + h_{x_{i-1}}^5}{h_{x_i} + h_{x_{i-1}}}\right).\end{aligned} \tag{2.7}$$

From equation (2.6), it is evident that

$$\begin{aligned}\partial_{xx}\phi_{i,j,k} = \delta_x\phi_{x_{i,j,k}} - \frac{1}{2}\left(h_{x_i} - h_{x_{i-1}}\right)\partial_{xxx}\phi_{i,j,k} - \frac{1}{6}\left(\frac{h_{x_i}^3 + h_{x_{i-1}}^3}{h_{x_i} + h_{x_{i-1}}}\right)\partial_{xxxx}\phi_{i,j,k} \\ - \frac{1}{24}\left(\frac{h_{x_i}^4 - h_{x_{i-1}}^4}{h_{x_i} + h_{x_{i-1}}}\right)\partial_{xxxxx}\phi_{i,j,k} + \mathcal{O}\left(\frac{h_{x_i}^5 + h_{x_{i-1}}^5}{h_{x_i} + h_{x_{i-1}}}\right).\end{aligned} \tag{2.8}$$

As our intention is to derive the generalized version of HOC formulation advocated in the work of Sen [130], we see from the above equations that the difference operator $(2\delta_x^2\phi_{i,j,k} - \delta_x\phi_{x_{i,j,k}})$ carries a first-order truncation error for the second-order derivative on nonuniform grid vis-a-vis its fourth-order truncation error in uniform grid and is given by

$$\partial_{xx}\phi_{i,j,k} = (2\delta_x^2\phi_{i,j,k} - \delta_x\phi_{x_{i,j,k}}) - \frac{1}{6}(h_{x_i} - h_{x_{i-1}})\partial_{xxx}\phi_{i,j,k} + \mathcal{O}\left(\frac{h_{x_i}^4 - h_{x_{i-1}}^4}{h_{x_i} + h_{x_{i-1}}}\right). \quad (2.9)$$

This necessitates a further approximation of $\partial_{xxx}\phi_{i,j,k}$ in equation (2.9) and is carried out using equation (2.6) to arrive at

$$\begin{aligned}\partial_{xx}\phi_{i,j,k} =& 2\left(\frac{h_{x_i}^2 - h_{x_i}h_{x_{i-1}} + h_{x_{i-1}}^2}{h_{x_i}^2 + h_{x_{i-1}}^2}(2\delta_x^2\phi_{i,j,k} - \delta_x\phi_{x_{i,j,k}})\right.\\ &\left. - \frac{h_{x_i} - h_{x_{i-1}}}{h_{x_i}^2 + h_{x_{i-1}}^2}(\delta_x\phi_{i,j,k} - \phi_{x_{i,j,k}})\right) + \frac{1}{12}(h_{x_i} - h_{x_{i-1}})^2\partial_{xxxx}\phi_{i,j,k}\\ &+ \mathcal{O}\left(\frac{(h_{x_i} - h_{x_{i-1}})(2h_{x_i}^4 - 2h_{x_i}^3h_{x_{i-1}} + 3h_{x_i}^2h_{x_{i-1}}^2 - 2h_{x_i}h_{x_{i-1}}^3 + 2h_{x_{i-1}}^4)}{(h_{x_i}^2 + h_{x_{i-1}}^2)}\right).\end{aligned} \quad (2.10)$$

The discretization of $\partial_{xx}\phi_{i,j,k}$ in equation (2.10) reports a only second-order truncation error on nonuniform grid but reverts to fourth-order accurate HOC scheme given in Sen [130] for uniform grids. As far as we are aware, it is the simplest generalization of Padé based compact scheme to nonuniform grids. Despite having second-order truncation accuracy, we advocate the above numerical discretization because of excellent numerical characteristics of $(2\delta_x^2\phi_{i,j,k} - \delta_x\phi_{x_{i,j,k}})$ in the context of CDE as documented earlier [130].

Analogously, along y- and z-direction we can approximate

$$\begin{aligned}\partial_{yy}\phi_{i,j,k} =& 2\left(\frac{h_{y_j}^2 - h_{y_j}h_{y_{j-1}} + h_{y_{j-1}}^2}{h_{y_j}^2 + h_{y_{j-1}}^2}(2\delta_y^2\phi_{i,j,k} - \delta_y\phi_{y_{i,j,k}})\right.\\ &\left. - \frac{h_{y_j} - h_{y_{j-1}}}{h_{y_j}^2 + h_{y_{j-1}}^2}(\delta_y\phi_{i,j,k} - \phi_{y_{i,j,k}})\right) + \frac{1}{12}(h_{y_j} - h_{y_{j-1}})^2\partial_{yyyy}\phi_{i,j,k}\\ &+ \mathcal{O}\left(\frac{(h_{y_j} - h_{y_{j-1}})(2h_{y_j}^4 - 2h_{y_j}^3h_{y_{j-1}} + 3h_{y_j}^2h_{y_{j-1}}^2 - 2h_{y_j}h_{y_{j-1}}^3 + 2h_{y_{j-1}}^4)}{(h_{y_j}^2 + h_{y_{j-1}}^2)}\right)\end{aligned} \quad (2.11)$$

and

$$\begin{aligned}\partial_{zz}\phi_{i,j,k} =& 2\left(\frac{h_{z_k}^2 - h_{z_k}h_{z_{k-1}} + h_{z_{k-1}}^2}{h_{z_k}^2 + h_{z_{k-1}}^2}(2\delta_z^2\phi_{i,j,k} - \delta_z\phi_{z_{i,j,k}})\right.\\ &\left. -\frac{h_{z_k} - h_{z_{k-1}}}{h_{z_k}^2 + h_{z_{k-1}}^2}(\delta_z\phi_{i,j,k} - \phi_{z_{i,j,k}})\right) + \frac{1}{12}(h_{z_k} - h_{z_{k-1}})^2\partial_{zzzz}\phi_{i,j,k}\\ &+ \mathcal{O}\left(\frac{(h_{z_k} - h_{z_{k-1}})(2h_{z_k}^4 - 2h_{z_k}^3h_{z_{k-1}} + 3h_{z_k}^2h_{z_{k-1}}^2 - 2h_{z_k}h_{z_{k-1}}^3 + 2h_{z_{k-1}}^4)}{(h_{z_k}^2 + h_{z_{k-1}}^2)}\right)\end{aligned} \tag{2.12}$$

respectively. The mixed derivatives can be approximated as

$$\begin{aligned}\partial_{xy}\phi_{i,j,k} =& \delta_x\phi_{y_{i,j,k}} + \delta_y\phi_{x_{i,j,k}} - \delta_x\delta_y\phi_{i,j,k} + \frac{1}{4}(h_{x_i} - h_{x_{i-1}})(h_{y_j} - h_{y_{j-1}})\partial_{xxyy}\phi_{i,j,k}\\ &+ \mathcal{O}\left(\frac{(h_{x_i}^3 + h_{x_{i-1}}^3)(h_{y_j} - h_{y_{j-1}})}{h_{x_i} + h_{x_{i-1}}}, \frac{(h_{x_i} - h_{x_{i-1}})(h_{y_j}^3 + h_{y_{j-1}}^3)}{h_{y_j} + h_{y_{j-1}}}\right),\end{aligned} \tag{2.13}$$

$$\begin{aligned}\partial_{yz}\phi_{i,j,k} =& \delta_y\phi_{z_{i,j,k}} + \delta_z\phi_{y_{i,j,k}} - \delta_y\delta_z\phi_{i,j,k} + \frac{1}{4}(h_{y_j} - h_{y_{j-1}})(h_{z_k} - h_{z_{k-1}})\partial_{yyzz}\phi_{i,j,k}\\ &+ \mathcal{O}\left(\frac{(h_{y_j}^3 + h_{y_{j-1}}^3)(h_{z_k} - h_{z_{k-1}})}{h_{y_j} + h_{y_{j-1}}}, \frac{(h_{y_j} - h_{y_{j-1}})(h_{z_k}^3 + h_{z_{k-1}}^3)}{h_{z_k} + h_{z_{k-1}}}\right)\end{aligned} \tag{2.14}$$

and

$$\begin{aligned}\partial_{zx}\phi_{i,j,k} =& \delta_z\phi_{x_{i,j,k}} + \delta_x\phi_{z_{i,j,k}} - \delta_z\delta_x\phi_{i,j,k} + \frac{1}{4}(h_{z_k} - h_{z_{k-1}})(h_{x_i} - h_{x_{i-1}})\partial_{zzxx}\phi_{i,j,k}\\ &+ \mathcal{O}\left(\frac{(h_{x_i} - h_{x_{i-1}})(h_{z_k}^3 + h_{z_{k-1}}^3)}{h_{z_k} + h_{z_{k-1}}}, \frac{(h_{x_i}^3 + h_{x_{i-1}}^3)(h_{z_k} - h_{z_{k-1}})}{h_{x_i} + h_{x_{i-1}}}\right).\end{aligned} \tag{2.15}$$

Having found the first-order, second-order and cross-derivative terms on nonuniform grids, we can express equation (2.3) around the central node (i, j, k) in the discrete form as follows,

$$[\mathscr{A}\phi]_{i,j,k} = f_{i,j,k}. \tag{2.16}$$

Here, the discrete operator $\mathscr{A}$ is defined as

$$
\begin{aligned}
[\mathscr{A}\phi]_{i,j,k} = &-\Bigg(2A_1\delta_x^2 + 2A_2\delta_y^2 + 2A_3\delta_z^2 + \frac{A_4}{h_{x_{i-1}}}\delta_x + \frac{A_5}{h_{y_{j-1}}}\delta_y + \frac{A_6}{h_{y_{j-1}}}\delta_z \\
&+ d_1\delta_x\delta_y + d_2\delta_y\delta_z + d_3\delta_z\delta_x\Bigg)\phi_{i,j,k} \\
&+ \left(A_1\delta_x + d_1\delta_y + d_3\delta_z + \frac{A_4}{h_{x_{i-1}}} + e_1\right)\phi_{x_{i,j,k}} \\
&+ \left(A_2\delta_y + d_1\delta_x + d_2\delta_z + \frac{A_5}{h_{y_{j-1}}} + e_2\right)\phi_{y_{i,j,k}} \\
&+ \left(A_3\delta_z + d_2\delta_y + d_3\delta_x + \frac{A_6}{h_{z_{k-1}}} + e_3\right)\phi_{z_{i,j,k}}
\end{aligned} \tag{2.17}
$$

where

$$
A_1 = \frac{2a_1(1-\alpha_x+\alpha_x^2)}{(1+\alpha_x^2)}, \quad A_2 = \frac{2a_2(1-\alpha_y+\alpha_y^2)}{(1+\alpha_y^2)}, \quad A_3 = \frac{2a_3(1-\alpha_z+\alpha_z^2)}{(1+\alpha_z^2)},
$$
$$
A_4 = \frac{2a_1(1-\alpha_x)}{(1+\alpha_x^2)}, \qquad A_5 = \frac{2a_2(1-\alpha_y)}{(1+\alpha_y^2)}, \qquad A_6 = \frac{2a_3(1-\alpha_z)}{(1+\alpha_z^2)}.
$$

The values of A_i, $i \in \{1, 2, \ldots, 6\}$, varies node to node in case of grids with nonregular spacings. Note that for uniform grids they remain fixed as α_x, α_y, and α_z remain constant throughout. Utilizing the operators δ_x, δ_y, δ_z, δ_x^2, δ_y^2, and δ_z^2 we achieve the following compact formulation for generalized 3D CDE (2.3) on a nineteen point stencil, shown in Fig. 2.1, as

$$
\sum_{l_x=-1}^{1}\sum_{l_y=-1}^{1}\sum_{l_z=-1}^{1} \widehat{A}_{i+l_x,j+l_y,k+l_z}\phi_{i+l_x,j+l_y,k+l_z} = F_{i,j,k}, \tag{2.18}
$$

with the coefficients

$$
\widehat{A}_{i,j,k} = 4\left(\frac{A_1}{\alpha_x h_{x_{i-1}}^2} + \frac{A_2}{\alpha_y h_{y_{j-1}}^2} + \frac{A_3}{\alpha_z h_{z_{k-1}}^2}\right)
$$
$$
\widehat{A}_{i+1,j,k} = -\frac{1}{h_{x_{i-1}}^2(1+\alpha_x)}\left(\frac{4A_1}{\alpha_x} + A_4\right), \quad \widehat{A}_{i-1,j,k} = -\frac{1}{h_{x_{i-1}}^2(1+\alpha_x)}\left(4A_1 + A_4\right),
$$
$$
\widehat{A}_{i,j+1,k} = -\frac{1}{h_{y_{j-1}}^2(1+\alpha_y)}\left(\frac{4A_2}{\alpha_y} + A_5\right), \quad \widehat{A}_{i,j-1,k} = -\frac{1}{h_{y_{j-1}}^2(1+\alpha_y)}\left(4A_2 + A_5\right),
$$
$$
\widehat{A}_{i,j,k+1} = -\frac{1}{h_{z_{k-1}}^2(1+\alpha_z)}\left(\frac{4A_3}{\alpha_z} + A_6\right), \quad \widehat{A}_{i,j,k-1} = -\frac{1}{h_{z_{k-1}}^2(1+\alpha_z)}\left(4A_3 + A_6\right),
$$
$$
\widehat{A}_{i-1,j+1,k} = \widehat{A}_{i+1,j-1,k} = -\widehat{A}_{i-1,j-1,k} = -\widehat{A}_{i+1,j+1,k} = \frac{d_1}{h_{x_{i-1}}h_{y_{j-1}}(1+\alpha_x)(1+\alpha_y)},
$$
$$
\widehat{A}_{i,j-1,k+1} = \widehat{A}_{i,j+1,k-1} = -\widehat{A}_{i,j+1,k+1} = -\widehat{A}_{i,j-1,k-1} = \frac{d_2}{h_{y_{j-1}}h_{z_{k-1}}(1+\alpha_y)(1+\alpha_z)},
$$
$$
\widehat{A}_{i+1,j,k-1} = \widehat{A}_{i-1,j,k+1} = -\widehat{A}_{i+1,j,k+1} = -\widehat{A}_{i-1,j,k-1} = \frac{d_3}{h_{x_{i-1}}h_{z_{k-1}}(1+\alpha_x)(1+\alpha_z)},
$$

and

$$
\begin{aligned}
F_{i,j,k} =& f_{i,j,k} - \left(\frac{A_4}{h_{x_{i-1}}} + c_1\right)\phi_{x_{i,j,k}} - \left(\frac{A_5}{h_{y_{j-1}}} + c_2\right)\phi_{y_{i,j,k}} - \left(\frac{A_6}{h_{z_{k-1}}} + c_3\right)\phi_{z_{i,j,k}}, \\
&- \frac{A_1}{h_{x_{i-1}}(1+\alpha_x)}\left(\phi_{x_{i+1,j,k}} - \phi_{x_{i-1,j,k}}\right) - \frac{d_1}{h_{y_{j-1}}(1+\alpha_y)}\left(\phi_{x_{i,j+1,k}} - \phi_{x_{i,j-1,k}}\right) \\
&- \frac{d_3}{h_{z_{k-1}}(1+\alpha_z)}\left(\phi_{x_{i,j,k+1}} - \phi_{x_{i,j,k-1}}\right) - \frac{A_2}{h_{y_{j-1}}(1+\alpha_y)}\left(\phi_{y_{i,j+1,k}} - \phi_{y_{i,j-1,k}}\right) \\
&- \frac{d_1}{h_{x_{i-1}}(1+\alpha_x)}\left(\phi_{y_{i+1,j,k}} - \phi_{y_{i-1,j,k}}\right) - \frac{d_2}{h_{z_{k-1}}(1+\alpha_z)}\left(\phi_{y_{i,j,k+1}} - \phi_{y_{i,j,k-1}}\right) \\
&- \frac{A_3}{h_{z_{k-1}}(1+\alpha_z)}\left(\phi_{z_{i,j,k+1}} - \phi_{z_{i,j,k-1}}\right) - \frac{d_2}{h_{y_{j-1}}(1+\alpha_y)}\left(\phi_{z_{i,j+1,k}} - \phi_{z_{i,j-1,k}}\right) \\
&- \frac{d_3}{h_{x_{i-1}}(1+\alpha_x)}\left(\phi_{z_{i+1,j,k}} - \phi_{z_{i-1,j,k}}\right).
\end{aligned}
$$

Equation (2.18) is the fully discretized compact scheme which is capable of solving the generalized 3D CDE on nonuniform grids. The scheme utilizes the values of the transport variable ϕ at nineteen neighboring points around the inner node (i, j, k) and the gradients of ϕ at six immediate neighbors denoted using red ink in Fig. 2.1. To the best of our knowledge, this is the first higher-order approximation that uses only nineteen grid points to approximate 3D CDE with mixed derivative and is a marked improvement from the pioneering work of Ananthakrishnaiah *et al.* [3]. Another potential advantage of this newly developed formulation is its suitability involving variable coefficients and even for semi-linear PDEs and will be further explored in numerical test cases. The gradients present in the discretization process need to be computed up to the desired order of accuracy. On a nonuniform grid, we generalize the idea of Lele [95] to arrive at the following approximation for spatial derivatives in x-direction,

$$
\begin{aligned}
\left(1 + \frac{h_{x_i}h_{x_{i-1}}}{6}\delta_x^2\right)\phi_{x_{i,j,k}} =& \left(\delta_x - \frac{h_{x_i} - h_{x_{i-1}}}{2}\delta_x^2\right)\phi_{i,j,k} \\
&+ \mathcal{O}\left((h_{x_i} - h_{x_{i-1}})(3h_{x_i}^2 + h_{x_i}h_{x_{i-1}} + 3h_{x_{i-1}}^2)\right).
\end{aligned} \tag{2.19}
$$

The truncation error term in the above approximation reveals an accuracy of order

three on nonuniform grids. Equation (2.19) can further be expanded to

$$\phi_{x_{i+1,j,k}}+2\left(1+\alpha_x\right)\phi_{x_{i,j,k}}+\alpha_x\phi_{x_{i-1,j,k}}=\frac{3}{\alpha_x h_{x_{i-1}}}\left(\phi_{i+1,j,k}-(1-\alpha_x^2)\phi_{i,j,k}-\alpha_x^2\phi_{i-1,j,k}\right). \tag{2.20}$$

Correspondingly, in y- and z-direction we get

$$\phi_{y_{i,j+1,k}}+2\left(1+\alpha_y\right)\phi_{y_{i,j,k}}+\alpha_y\phi_{y_{i,j-1,k}}=\frac{3}{\alpha_y h_{y_{j-1}}}\left(\phi_{i,j+1,k}-(1-\alpha_y^2)\phi_{i,j,k}-\alpha_y^2\phi_{i,j-1,k}\right) \tag{2.21}$$

and

$$\phi_{z_{i,j,k+1}}+2\left(1+\alpha_z\right)\phi_{z_{i,j,k}}+\alpha_z\phi_{z_{i,j,k-1}}=\frac{3}{\alpha_z h_{z_{k-1}}}\left(\phi_{i,j,k+1}-(1-\alpha_z^2)\phi_{i,j,k}-\alpha_z^2\phi_{i,j,k-1}\right) \tag{2.22}$$

respectively.

2.3 Solution of algebraic systems of equations

The system of equations resulting from the newly developed FD scheme (2.18) can be written in matrix form as

$$M_1\Phi=F_1(f,\Phi_x,\Phi_y,\Phi_z), \tag{2.23}$$

with

$$\begin{aligned}
\Phi &= \left(\phi_{1,1,1},\phi_{1,1,2},\ldots,\phi_{1,1,n_z},\phi_{1,2,1},\phi_{1,2,2},\ldots,\phi_{1,n_y,n_z},\ldots,\phi_{n_x,n_y,n_z}\right)^T,\\
\Phi_x &= \left(\phi_{x_{1,1,1}},\phi_{x_{1,1,2}},\ldots,\phi_{x_{1,1,n_z}},\phi_{x_{1,2,1}},\phi_{x_{1,2,2}},\ldots,\phi_{x_{1,n_y,n_z}},\ldots,\phi_{x_{n_x,n_y,n_z}}\right)^T,\\
\Phi_y &= \left(\phi_{y_{1,1,1}},\phi_{y_{1,1,2}},\ldots,\phi_{y_{1,1,n_z}},\phi_{y_{1,2,1}},\phi_{y_{1,2,2}},\ldots,\phi_{y_{1,n_y,n_z}},\ldots,\phi_{y_{n_x,n_y,n_z}}\right)^T,
\end{aligned}$$

and

$$\Phi_z = \left(\phi_{z_{1,1,1}},\phi_{z_{1,1,2}},\ldots,\phi_{z_{1,1,n_z}},\phi_{z_{1,2,1}},\phi_{z_{1,2,2}},\ldots,\phi_{z_{1,n_y,n_z}},\ldots,\phi_{z_{n_x,n_y,n_z}}\right)^T,$$

where M_1 is a sparse nonsymmetric matrix of dimension $n_xn_yn_z$. Nonsymmetricity being correlated by the nonuniform grids taken under application. Moreover, due to compactness of the presented scheme, M_1 is a banded matrix with nineteen diagonals.

The solution for steady-state generalized CDE (2.18) is computed following an outer-inner iterative technique. Once Φ is initialised appropriately, we approximate Φ_x, Φ_y and Φ_z by solving the following tri-diagonal systems of equations

$$M_2\Phi_x = F_2(\Phi), \tag{2.24}$$

$$M_3\Phi_y = F_3(\Phi) \tag{2.25}$$

and

$$M_4\Phi_z = F_4(\Phi) \tag{2.26}$$

respectively. Equations (2.24)–(2.26) are the matrix reperentation of equations (2.20)–(2.22). We thus obtain the required initial values and use equation (2.23) towards first iteration $\Phi^{(1)}$ of Φ. This is followed by computation of $\Phi_x^{(1)}$, $\Phi_y^{(1)}$ and $\Phi_z^{(1)}$ leading to completion of one outer iteration. We begin the next outer iteration by utilizing these values on the right hand side of equation (2.23) to compute Φ again. The process continues unless the following condition is reached:

$$max|\Phi_{i,j,k}^{(n+1)} - \Phi_{i,j,k}^{(n)}| < \epsilon_1,$$

where $\Phi_{i,j,k}^{(n+1)}$ and $\Phi_{i,j,k}^{(n)}$ are the values of Φ computed at two successive outer iterations.

An outer iteration involves the solution of as many as four systems of equations given in equations (2.23)–(2.26). Each system of equations is handled by an iterative solver. The Bi-Conjugate Gradient Stabilized (BiCGstab) method [83] is used to perform all the inner computations. The tolerance criteria for inner iterations is set to ϵ_2. In our computations we recommend $\epsilon_1 = \epsilon_2 = 1.0e - 14$. It is important to mention that under-relaxation was used in the inner iterations for a low diffusive coefficient. All computations are executed on a Intel i7 based PC with 2.40 GHz CPU and 16 GB RAM.

2.4 Grid generation

To test our newly developed discretization strategy, we have adopted two different types of nonuniform grids: (i) geometrically generated and (ii) trigonometrically generated and are extensively used in numerical examples.

For the first scenario, we use the nonuniform grid that stretches geometrically in all the three direction. The grid is generated with the help of algebraic relation

$$x_i = X_0 \left[\frac{\alpha_x^{(i-1)} - 1}{\alpha_x - 1} \right], \quad y_j = Y_0 \left[\frac{\alpha_y^{(j-1)} - 1}{\alpha_y - 1} \right], \quad z_k = Z_0 \left[\frac{\alpha_z^{(k-1)} - 1}{\alpha_z - 1} \right], \tag{2.27}$$

with X_0, Y_0 and Z_0 being the initial spacings in x-, y- and z-direction respectively.

In the second case, a nonuniform grid is generated using trigonometric functions given below:

$$\begin{aligned} x_i &= L_x \left\{ \frac{i}{n_x} + \frac{\lambda_x}{\Theta_x} \sin\left(\frac{\Theta_x i}{n_x} \right) \right\}, \\ y_j &= L_y \left\{ \frac{j}{n_y} + \frac{\lambda_y}{\Theta_y} \sin\left(\frac{\Theta_y j}{n_y} \right) \right\}, \\ z_k &= L_z \left\{ \frac{k}{n_z} + \frac{\lambda_z}{\Theta_z} \sin\left(\frac{\Theta_z k}{n_z} \right) \right\}, \quad -1 \leq \lambda_x, \lambda_y, \lambda_z \leq 1. \end{aligned} \tag{2.28}$$

Here, L_x, λ_x and Θ_x respectively defines length of the domain, the clustering parameters and control angle along the x-direction. The control angle decides the area which requires grid refinement and the clustering parameter controls the density of grids in that area. Positive values of λ_x correspond to the clustering of grids in the required zone while the negative value defines the otherwise. It should be noted that the zero value of the clustering parameter restores to uniform grids. The parameters L_y, L_z, λ_y, λ_z, Θ_y and Θ_z carries the same significance in the y- and z-directions.

For problems with solutions containing steep boundary layers, we shall adopt the trigonometrically generated grid as it allows us to accumulate more number of grids in the required region compared to the geometric one as can be seen in Fig. 2.2. Moreover, for the second type of grids, bigger values of α_x, α_y and α_z lead to a quick exponential increase of grid spacings.

Gird generations carried out using equations (2.27) and (2.28) can also be used as transformations from physical to computational domain. The effect of such grid

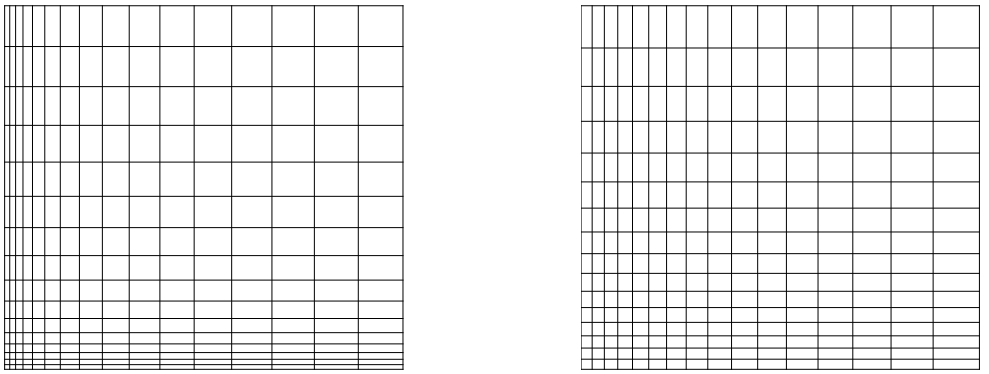

(a) (b)

Fig. 2.2: Nonuniform grid distribution on xy-plane for a $17\times17\times17$ grid : (a) triginometrically generated with $\lambda_x = \lambda_y = -0.8$ and (b) geometrically generated with $\alpha_x = \alpha_y = 1.1$.

stretching on the stability and accuracy in generalized setup for higher-order compact schemes vis-à-vis higher-order discretization directly applied to the stretched physical grid without using the coordinate transformation have been well documented in the work of Zhong [186]. Such a study in the context of 3D generalized CDE might be revisited in the future but is avoided in the current context.

2.5 Numerical illustrations

In this section, we employ eight numerical test cases to examine the newly developed compact scheme articulated in this chapter. They exhibit the effectiveness, accuracy, convergence order and adaptivity of the scheme for various 2D and 3D linear and nonlinear PDEs, including singularly perturbed problems with boundary layer as well as elliptic PDEs with mixed derivatives. A detailed analysis of our computed results along with a comprehensive comparison to those available in the literature is carried out.

All the test initializations are done with zero value. Although for steady-state problems at times, it is preferable to work with an initial approximation closer to the exact solution to assure the convergence, it is heartening to say that the zero initial guesses have worked fine for all the test problems under consideration. The

numerical rate of convergence for each problem is to calculate with the help of the following definition:

$$\text{Order of convergence} = \frac{\log\left(\mathscr{E}^{H_1}/\mathscr{E}^{H_2}\right)}{\log(H_2/H_1)}, \tag{2.29}$$

where $\mathscr{E}^{H_1}$ and $\mathscr{E}^{H_2}$ are the maximum error of the solution with total grid points H_1 and H_2 respectively.

2.5.1 Test problem 1

We begin our numerical test cases with the following 2D homogeneous linear elliptic PDE

$$\frac{\partial^2\phi}{\partial x^2} + \frac{\partial^2\phi}{\partial y^2} + c\frac{\partial\phi}{\partial x} = 0, \qquad 0 \leq x, y \leq 1. \tag{2.30}$$

This equation admits exact solution

$$\phi(x, y) = \left(y(1-y) - \frac{2x}{c}\right) e^{-cx} \tag{2.31}$$

with a vertical boundary layer at $x = 0$ as noted by Tian *et al.* [156]. With increasing c, this boundary layer gets narrower. Thus, any effective capture of this vertical layer necessitates nonuniform grid distribution in the x-direction, with clustering in the vicinity of $x = 0$. We thus put our numerical scheme to the test by varying the stretching parameters while laying a uniform grid in the conjugate y-direction. Computations are performed using grids of various sizes and stretching parameters, with the Dirichlet boundary condition applied along both sides. Maximum error corresponding to $c = 10^3$ and 10^4 are plotted in Fig. 2.3a and 2.3b respectively. From the Fig. 2.3a and 2.3b, it is clear that for a particular value of λ_x, inaccuracy decreases as the number of grid points increases. Alternatively, error reduction can be accomplished by carefully raising the magnitude of λ_x, which has been shown to be highly effective. This documents the efficiency of the nonuniform grids advocated in this study.

Following Tian *et al.* [156], further computations for this problem are performed with $c = 10$, 10^2, 10^3 and 10^4. This allows us to compare our newly developed method to the best accessible in the literature. In Table 2.1, the maximum errors

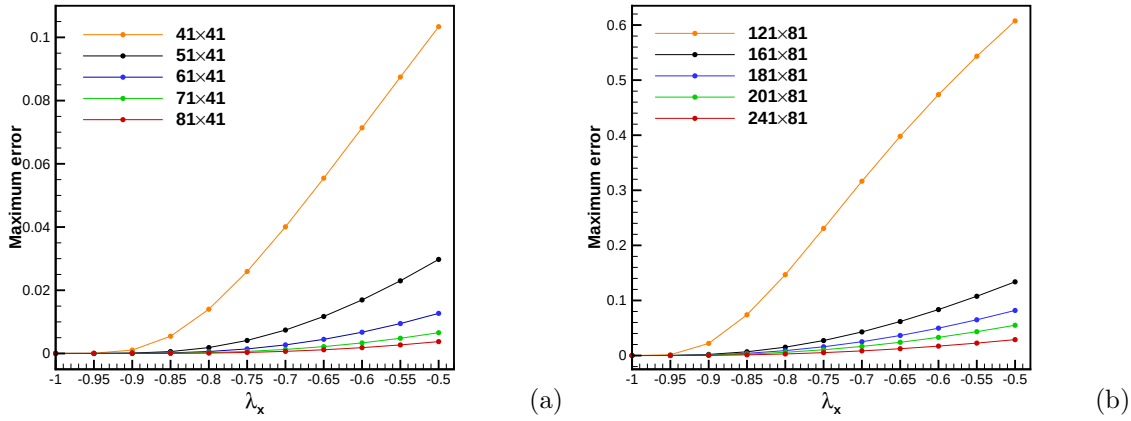

Fig. 2.3: Problem 1: Maximum error vs stretching parameter for different grid sizes: (a) $c = 10^3$ and (b) $c = 10^4$.

Table 2.1: Test problem 1: Maximum error of ϕ for different scheme on grids of different sizes and order of convergence.

	Grid size	[156]		Present scheme	
		Max. error	order	Max. error	order
$c = 10$	21×21	3.94e-6		3.77e-6	
$\lambda_x = -0.30$	41×41	2.46e-7	4.00	2.52e-7	3.90
$c = 10^2$	21×21	2.54e-5		5.40e-5	
$\lambda_x = -0.85$	41×41	1.50e-6	4.09	3.65e-6	3.89
$c = 10^3$	41×21	4.40e-5		9.00e-5	
$\lambda_x = -0.95$	81×41	2.40e-6	4.19	5.08e-6	4.15
$c = 10^4$	121×41	7.45e-6		6.22e-6	
$\lambda_x = -1.00$	241×81	4.44e-7	4.07	4.03e-7	3.95

of the computed solutions are shown. In this table, we also present errors reported by the compact scheme of Tian *et al.* [156]. Though the newly developed scheme has a theoretical accuracy of second order, the order of convergence was observed to gravitate to the highest attainable order four in each case. Additionally, we can observe that the present scheme is quite suitable in capturing extremely thin boundary layers with equivalent efficiency as that of Tian *et al.* [156].

2.5.2 Test problem 2

The course of this study is furthered by resolving boundary layers of the following PDE in the presence of mixed derivative

$$-\left(\frac{\partial^2\phi}{\partial x^2}+\frac{\partial^2\phi}{\partial y^2}\right)+b\frac{\partial^2\phi}{\partial x\partial y}-c\left(\frac{\partial\phi}{\partial x}-\frac{\partial\phi}{\partial y}\right)=f(x,y),\quad 0\leq x,y\leq 1. \tag{2.32}$$

Here, $|b|<2$ and the exact solution of this elliptic PDE is given by

$$\phi(x,y)=\frac{e^{c(1-x)}+e^{cy}-2}{e^{c}-1}. \tag{2.33}$$

Equation (2.33) helps in determining the source function $f(x,y)$ and the Dirichlet boundary conditions [42]. The analytical solution admits vertical boundary layers along $x=0$ and $y=1$. As recognized by Fournié and Karaa [42], the boundary layer thickness changes inversely with c, making accurate resolution of the same exceedingly demanding. Another issue for any discretization is the question of convergence as $|b|$ assume values close to 2. The stability of diversified discretization near and beyond such a choice is well documented in [42]. As $b\to 2$, the associated diffusion matrix tends to lose positive definiteness and the nature of the PDE in equation (2.32) becomes parabolic. Thus, testing our newly developed discretization, particularly with larger c at a steep b value, should be interesting. We start by considering a suitable nonuniform grid capable in capturing the boundary layers by using the stretching function (2.28) with $\Theta_x=-\Theta_y=\pi$.

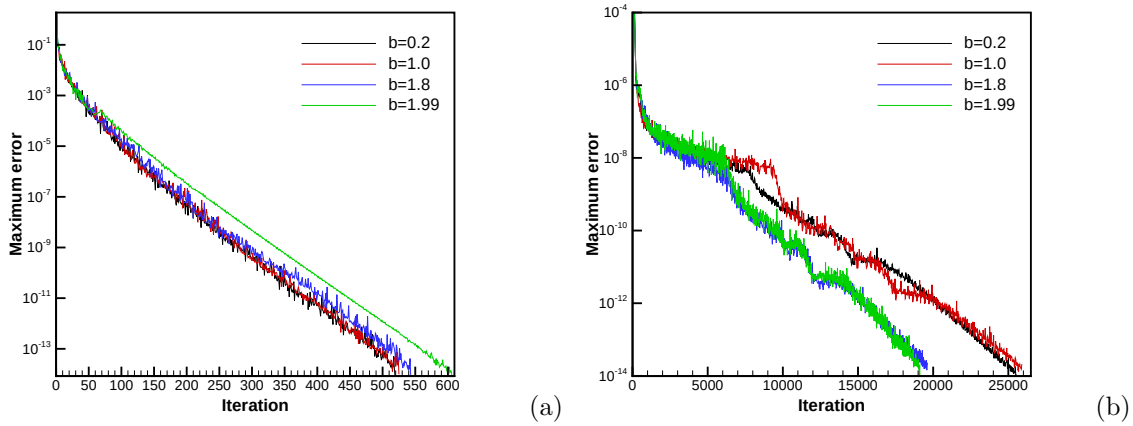

Fig. 2.4: Problem 2: Maximum error versus iteration numbers: (a) $c=10^3$ and (b) $c=10^4$.

Table 2.2: Test problem 2: Comparison of maximum error and order of convergence of different methods, $1 \leq c \leq 10^3$.

c	[42]			Present Scheme			
	65×65	order	129×129	65×65	order	129×129	λ
			$b = 0.2$				
1	1.19e-11	5.18	3.28e-13	8.34e-12	3.83	5.85e-13	0.10
10	4.85e-7	4.00	3.03e-8	8.29e-8	3.99	5.22e-9	0.65
10^2	5.45e-3	4.12	3.12e-4	3.63e-6	3.99	2.29e-7	0.95
10^3	6.73e-1	0.92	3.55e-1	5.29e-5	3.94	3.45e-6	0.99
			$b = 1.0$				
1	1.26e-11	4.01	7.80e-13	8.51e-12	3.89	5.76e-13	0.10
10	4.88e-7	4.00	3.05e-8	8.86e-8	3.99	5.59e-9	0.65
10^2	5.35e-3	4.18	3.06e-4	3.65e-6	3.98	2.31e-7	0.95
10^3	6.57e-1	0.95	3.41e-1	5.28e-5	3.94	3.45e-6	0.99
			$b = 1.8$				
1	1.54e-11	4.21	8.27e-13	9.48e-12	3.94	6.16e-13	0.10
10	5.26e-7	4.00	3.28e-8	1.03e-7	3.99	6.49e-9	0.65
10^2	5.54e-3	4.05	3.34e-4	3.69e-6	3.99	2.33e-7	0.95
10^3	6.64e-1	1.01	3.30e-1	5.27e-5	3.93	3.45e-6	0.99
			$b = 1.99$				
1	–	–	–	1.01e-11	3.84	7.03e-13	0.10
10	–	–	–	1.09e-7	3.99	6.87e-9	0.65
10^2	–	–	–	3.70e-6	3.98	2.34e-7	0.95
10^3	–	–	–	5.28e-5	3.94	3.45e-6	0.99

Table 2.3: Test problem 2: Maximum error and order of convergence for $c = 10^4$.

Grid	$b = 0.2$	$b = 1.0$	$b = 1.8$	$b = 1.99$
129×129	7.71e-5	7.71e-5	7.71e-5	7.71e-5
257×257	5.33e-6	5.33e-6	5.41e-6	5.41e-6
order	3.84	3.84	3.83	3.83

Fournié and Karaa [42] solved this problem on a uniform grid with a generalized nine-point fourth-order compact formulation. The scheme generated by them outperformed the traditional central difference method in terms of accuracy and convergence of the solution. A close comparison of the solutions computed by Fournié and Karaa [42] and the present scheme has been shown Table 2.2. Both the schemes

could properly tackle the issues associated with boundary layers and numerical oscillations for $c \leq 100$. In this context, the current formulation, which similarly employes nine-point stencil in two dimensions, reports better accuracy as it is proficient in dealing with nonuniform grid generated using $\lambda_x = \lambda_y = \lambda$. However, for $c = 10^3$ the compact approach established in [42] cannot maintain the requisite accuracy and convergence. We further probe the newly developed formulation for convection coefficient $c = 10^4$ using the finer grid and report results in Table 2.3. Our newly developed formulation is again found to be efficient in capturing the narrow boundary layers and reports higher than the theoretical order of convergence.

The convergence history for $c = 10^3$ and 10^4 are presented in Fig. 2.4a and 2.4b respectively. It is seen that on a 129×129 grid, variation of b has little effect on the convergence pattern. The correlation between the number of iterations and b remains undetermined as c is increased to 10^4. This might be attributed to the nonuniform grid's ability to resolve boundary layers effectively. Note that working with a uniform grid Fournié and Karaa [42] demonstrated that with an increase in b more iterations are necessary to achieve convergence.

2.5.3 Test problem 3

We next pass on to three dimensional test cases and consider the CDE

$$-\varepsilon\left(\frac{\partial^2\phi}{\partial x^2}+\frac{\partial^2\phi}{\partial y^2}+\frac{\partial^2\phi}{\partial z^2}\right)+\frac{1}{1+y}\frac{\partial\phi}{\partial y}=f(x,y,z),\quad 0\leq x,y,x\leq 1. \tag{2.34}$$

The exact solution of this equation is

$$\phi(x,y,z)=z\left(e^{y-x}+2^{-\frac{1}{\varepsilon}}(1+y)^{1+\frac{1}{\varepsilon}}\right). \tag{2.35}$$

Here, the Dirichlet boundary conditions and the source function $f(x,y,z)$ are generated from equation (2.35). This problem was studied by Ge and Zhang [48] and Mohamed *et al.* [103] using uniform grids. The problem admits a steep boundary layer at $y = 1$ for large value of $1/\varepsilon$. We use the stretching function given in equation (2.28) to lay out a nonuniform grid with clustering near $y = 1$ to evaluate the efficiency of our discretization scheme in a nonuniform setup.

Ensuring the work done by Mohamed *et al.* [103], we carried out the computa-

Table 2.4: Test problem 3: Comparison of maximum error and order of convergence of different schemes for different ε.

	Grid size	[103]		[48]		Present scheme	
		Max. error	order	Max. error	order	Max. error	order
$\varepsilon = 1.00$	$7 \times 7 \times 7$	1.94e-7		4.74e-7		1.89e-8	
$\lambda_y = 0.10$	$11 \times 11 \times 11$	3.25e-8	3.95	8.32e-8	3.85	2.84e-9	3.71
	$21 \times 21 \times 21$	2.07e-9	3.96	5.25e-9	3.99	2.12e-10	3.74
	$41 \times 41 \times 41$	1.29e-10	4.00	3.31e-10	3.99	1.48e-11	3.84
$\varepsilon = 0.10$	$7 \times 7 \times 7$	8.13e-5		2.32e-4		5.08e-5	
$\lambda_y = 0.40$	$11 \times 11 \times 11$	1.42e-5	3.86	3.88e-5	3.96	7.29e-6	3.80
	$21 \times 21 \times 21$	8.91e-7	3.99	2.40e-6	4.00	4.89e-7	3.90
	$41 \times 41 \times 41$	5.58e-8	4.00	1.50e-7	4.00	3.16e-8	3.95
$\varepsilon = 0.01$	$11 \times 11 \times 11$	1.27e-3		1.71e-1		1.93e-3	
$\lambda_y = 0.85$	$21 \times 21 \times 21$	7.02e-4	0.78	2.90e-2	2.56	7.12e-5	4.76
	$41 \times 41 \times 41$	8.58e-5	3.03	2.48e-3	3.54	4.65e-6	3.94

tions for $\varepsilon = 1$, 0.1 and 0.01. Table 2.4 shows the accuracy and convergence of the current scheme. The numerical results of the present scheme are compared to results obtained with a discretization strategy developed by Ge and Zhang [48] with the help of symbolic computations and exponential HOC scheme proposed by Mohamed *et al.* [103]. Both these schemes being limited to uniform meshes only, a superior performance of the present scheme is noticed in Table 2.4. For higher ε values, all three approaches exhibit satisfactory results in terms of accuracy and convergence in case of gentle boundary layers. However, the present scheme maintains a convergence near to fourth-order as the boundary layer becomes thinner. Furthermore, for all the values of ε the present scheme shows notably higher accuracy than the other two.

2.5.4 Test problem 4

Next, we apply our methodology on the linear CDE whose coefficients are exponential functions of spatial coordinates in the cubic domain $[0, 1]^3$ represented by

$$e^{2x}\frac{\partial^2\phi}{\partial x^2}+e^{2y}\frac{\partial^2\phi}{\partial y^2}+e^{2z}\frac{\partial^2\phi}{\partial z^2}+e^{(x+y+z)}\left(\frac{\partial\phi}{\partial x}+\frac{\partial\phi}{\partial y}+\frac{\partial\phi}{\partial z}\right)=f(x,y,z). \quad (2.36)$$

The equation admits exact solution

$$\phi(x,y,z)=\cos(x)+\cos(y)+\cos(z) \quad (2.37)$$

and is traditionally used by various researchers as a numerical test for three-dimensional code verification [3, 4, 105]. Indeed the problem was studied by Ananthakrishnaiah *et al.* in their classical work [3]. Later Mohanty and Setia solved this linear problem to establish a fourth-order compact off-step discretization in their work [105]. Recently Aziz *et al.* [4] while introducing a Haar wavelet-based method again took recourse to this problem. Our aim here is to compare the computational effectiveness of the newly developed discretization with a fast second-order central difference approximation in addition to measuring the accuracy of the proposed discretization.

Table 2.5: Test problem 4: Comparisons of maximum error and order of convergence of different schemes.

Grid size	[3]		[105]		[4]		Present scheme	
	Max. error	order	Max. error	order	Max. error	order	Max. error	order
$5\times5\times5$	8.88e-5		2.63e-5		1.06e-4		2.11e-7	
$9\times9\times9$	5.18e-6	4.10	1.65e-6	3.99	3.34e-5	1.67	1.25e-8	4.08
$17\times17\times17$	3.18e-7	4.03	1.03e-7	4.00	8.52e-6	1.97	8.02e-10	3.96

We refrain from employing nonuniform meshes because the exact solution (2.37) carries symmetry and smoothness in all directions. This also provides us with an opportunity to check whether the discretization is able to report close to its highest possible order of convergence. In keeping with the literature, we also compare maximum error on grids $5\times5\times5$, $9\times9\times9$ and $17\times17\times17$ with classical works in Table 2.5. The extinguishing performance of our newly developed formulation becomes apparent from this table as well. It is imperative to mention that the results obtained by the present scheme remain more accurate compared to results obtained by the central schemes available in the literature. The fourth-order convergence in the uniform grid is indeed reported by the current approach, as shown in Table 2.5.

2.5.5 Test problem 5

We now investigate our scheme for homogeneous CDE in presence of mixed derivatives given by

$$-\nabla \cdot (\boldsymbol{D}\nabla\phi) + \nabla \cdot (\boldsymbol{C}\phi) = 0 \tag{2.38}$$

where

$$\boldsymbol{D} = \varepsilon \begin{bmatrix} 2 & -b & b \\ -b & 2 & -b \\ b & -b & 2 \end{bmatrix},$$

$$\boldsymbol{C} = \left[-2\tanh\left(\tfrac{x-0.5}{2\varepsilon}\right), -2\tanh\left(\tfrac{y-0.5}{2\varepsilon}\right), -2\tanh\left(\tfrac{z-0.5}{2\varepsilon}\right)\right]^T.$$

Here, b conforms the positive definiteness of $\boldsymbol{D}$ and the Dirichlet boundary conditions conform to the exact solution

$$\phi(x,y,z) = -\tanh\left(\frac{x-0.5}{2\varepsilon}\right) - \tanh\left(\frac{y-0.5}{2\varepsilon}\right) - \tanh\left(\frac{z-0.5}{2\varepsilon}\right) \tag{2.39}$$

which admits three vertical boundary layers along $x = 0.5$, $y = 0.5$ and $z = 0.5$. Our goal in this particular problem is to evaluate the efficiency of the discretization approach for various values of b within the allowable range. In terms of computational time, we also compare our method with the traditional second-order central difference method using $\varepsilon = 0.5$ and 0.05. All the computations are done on a centrosymmetric nonuniform grid generated using equation (2.28) with $\Theta_x = \Theta_y = \Theta_z = 2\pi$. Solutions computed for $b = 0.5$, 1.0, 1.2 and 1.6 using three different grids $9 \times 9 \times 9$, $17 \times 17 \times 17$ and $33 \times 33 \times 33$ are shown in Table 2.6. The relative CPU time of our recently established scheme and that of a second-order central scheme, which requires less computing, is also reported in this table.

Table 2.6 shows that the second-order central scheme is nearly six times faster than our recently proposed formulation for smaller b values at $\varepsilon = 0.5$. With boundary layers becoming steep at $\varepsilon = 0.05$, this discrepancy in CPU time is substantially evened out. This is attributed to the large number of iterations required by the central scheme for convergence. The central scheme is inefficient in terms of computational cost and accuracy for $b = 1.6$ and struggles to converge even for the case

Table 2.6: Test problem 5: Comparisons of maximum error, order of convergence and relative CPU time.

ε	β	Grid size	Central scheme			Present scheme		
			Max. error	order	Time	Max. error	order	Time
0.5	0.5	$9 \times 9 \times 9$	3.53e-5		1	3.75e-7		4.9
		$17 \times 17 \times 17$	9.85e-6	1.84	10.4	2.83e-8	3.73	63
		$33 \times 33 \times 33$	2.53e-6	1.96	221	1.90e-9	3.90	1333.3
	1.0	$9 \times 9 \times 9$	4.20e-5		1.9	4.37e-7		5.7
		$17 \times 17 \times 17$	1.21e-5	1.80	12.5	3.11e-8	3.81	76.3
		$33 \times 33 \times 33$	3.16e-6	1.94	285.6	2.02e-9	3.94	1614
	1.2	$9 \times 9 \times 9$	4.70e-5		1.6	4.66e-7		6
		$17 \times 17 \times 17$	1.56e-5	1.59	25.1	3.24e-8	3.85	82
		$33 \times 33 \times 33$	–	–	–	2.08e-9	3.96	1705.3
	1.6	$9 \times 9 \times 9$	1.64e-4		16186.6	5.31e-7		6
		$17 \times 17 \times 17$	–	–	–	3.54e-8	3.85	96
		$33 \times 33 \times 33$	–	–	–	2.21e-9	3.96	2032.4
0.05	0.5	$9 \times 9 \times 9$	2.16e-2		18.1	3.96e-3		19.4
		$17 \times 17 \times 17$	5.91e-3	1.87	159.5	3.02e-4	3.71	154.2
		$33 \times 33 \times 33$	1.52e-3	1.96	2172.8	1.98e-5	3.93	1683.4
	1.0	$9 \times 9 \times 9$	2.20e-2		19.4	4.00e-3		20
		$17 \times 17 \times 17$	5.98e-3	1.88	160.7	3.04e-4	3.72	167.7
		$33 \times 33 \times 33$	1.54e-3	1.96	1916.6	2.00e-5	3.93	1754.5
	1.2	$9 \times 9 \times 9$	2.21e-2		23	4.02e-3		20.7
		$17 \times 17 \times 17$	6.02e-3	1.88	158.2	3.05e-4	3.72	176.8
		$33 \times 33 \times 33$	1.55e-3	1.96	2419	2.00e-5	3.93	1980.5
	1.6	$9 \times 9 \times 9$	–		–	4.07e-3		21.4
		$17 \times 17 \times 17$	–	–	–	3.07e-4	3.73	193.7
		$33 \times 33 \times 33$	–	–	–	2.01e-5	3.93	2275.2

$\varepsilon = 0.5$. In terms of maximum error, the Table 2.6 clearly shows that the newly proposed formulation attains close to fourth-order convergence.

In Fig. 2.5, a qualitative comparison of the present numerical solution and the exact solution is carried out. It is encouraging to see that the solution computed on a $33 \times 33 \times 33$ grid on the plane $y = 0.5$ for $\varepsilon = 0.05$ is essentially identical to analytical solution.

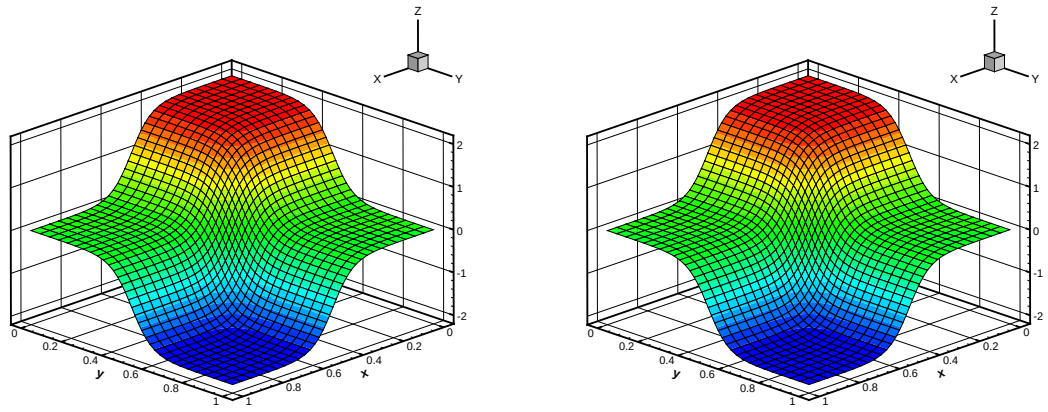

(a) (b)

Fig. 2.5: Problem 5: (a) Computed solution and (b) analytical solution on the plane $y = 0.5$ for $\varepsilon = 0.05$ on $33 \times 33 \times 33$ grid.

2.5.6 Test problem 6

Next, we solve the nonlinear elliptic PDE on a unit cube using the present method. The nonlinear equation

$$\frac{\partial^2 \phi}{\partial x^2} + \frac{\partial^2 \phi}{\partial y^2} + \frac{\partial^2 \phi}{\partial z^2} - \phi \left(\frac{\partial \phi}{\partial x} + \frac{\partial \phi}{\partial y} + \frac{\partial \phi}{\partial z} \right) = f(x, y, z) \tag{2.40}$$

with source term $f(x, y, z)$ possesses analytic solution

$$\phi(x, y, z) = z e^{(1-x)(1-y)/\varepsilon}. \tag{2.41}$$

Table 2.7: Test problem 6: Computed maximum error and order of convergence for different ε.

Grid size	$\varepsilon = 1$		$\varepsilon = 10^{-1}$		$\varepsilon = 10^{-2}$		$\varepsilon = 5 \times 10^{-3}$	
	$\lambda = 0.00$		$\lambda = 0.40$		$\lambda = 0.85$		$\lambda = 0.95$	
	Max error	order	Max error	order	Max error	order	Max error	order
$9 \times 9 \times 9$	1.15e-9		4.99e-6		1.07e-3		–	
$17 \times 17 \times 17$	8.86e-11	3.70	4.83e-7	3.37	8.95e-5	3.58	7.40e-4	–
$25 \times 25 \times 25$	1.87e-11	3.84	1.10e-7	3.65	1.93e-5	3.78	1.72e-4	3.60
$33 \times 33 \times 33$	6.08e-12	3.91	3.75e-8	3.74	6.37e-6	3.85	5.85e-5	3.75
$41 \times 41 \times 41$	2.49e-12	4.00	1.60e-8	3.82	2.67e-6	3.90	2.49e-5	3.83

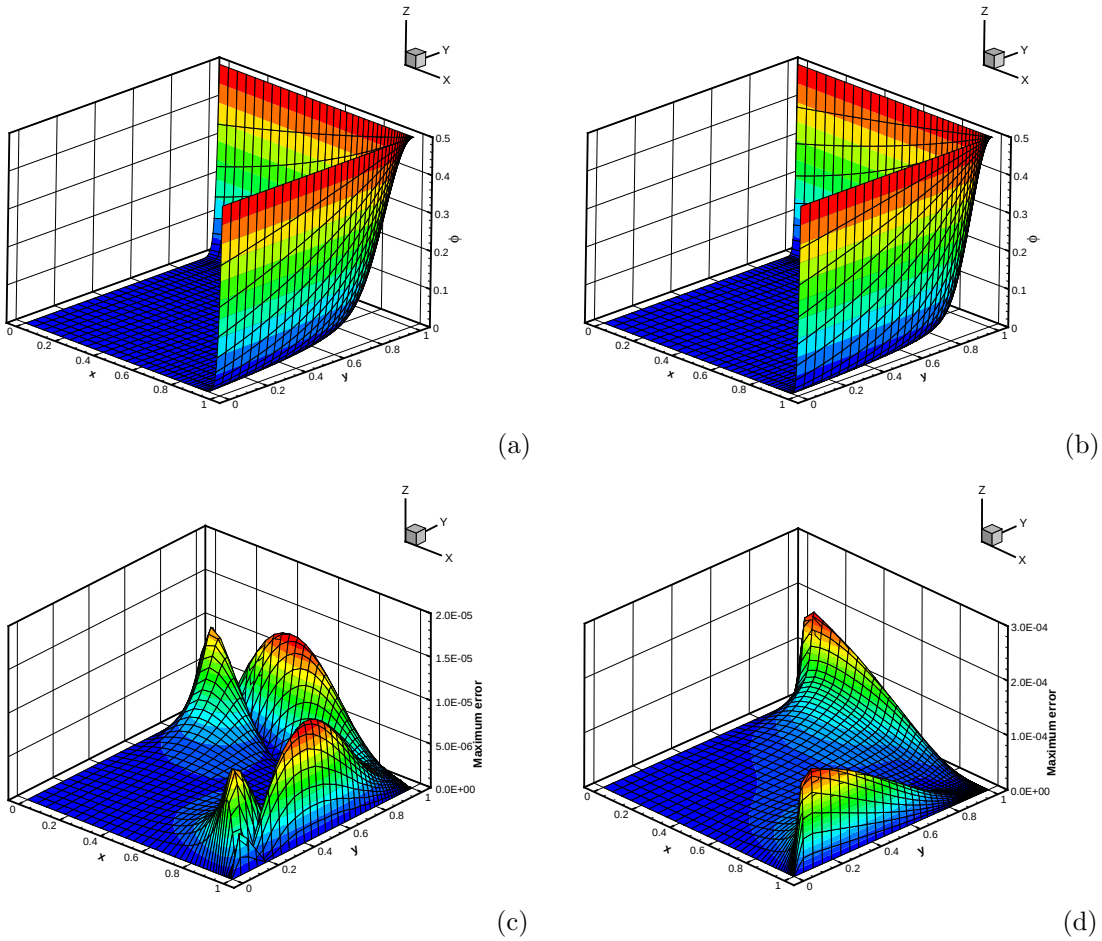

Fig. 2.6: Problem 6: Numerical solution ((a) and (b)) and maximum error ((c) and (d)) on the plane $z = 0.5$ computed using $41 \times 41 \times 41$ grid for $\varepsilon = 0.01$ (left) and $\varepsilon = 0.005$ (right).

For smaller values of ε, this solution develops two vertical layers along the boundaries $x = 1$ and $y = 1$ respectively. In order to properly capture the solution, it is essential to generate nonuniform grids along the x- and y-directions, and a uniform grid in the z-direction. Grids are clustered in the vicinity of $x = 1$ and $y = 1$ using equation (2.28), with the grid stretching function being $\Theta_x = \Theta_y = \pi$. Computations are carried up to $\varepsilon = 5.0e - 3$. We obtain a smooth solution for $\varepsilon = 1$ that is successfully handled by uniform grids in all directions. However, it becomes more challenging to capture the boundary layers of the nonlinear equation for smaller values of ε. For each value of ε we have chosen different clustering parameter $\lambda_x = \lambda_y = \lambda$ which can be seen in Table 2.7. This table clearly shows that the newly developed scheme is able to sustain its theoretical rate of convergence and

accuracy for this nonlinear problem, thereby affirming the adaptivity of the present scheme in simulating challenging situations. Finally, numerical solution on the plane $z = 0.5$ computed using $41 \times 41 \times 41$ grid for $\varepsilon = 0.01$ and $\varepsilon = 0.005$ are presented in Fig. 2.6a and 2.6b respectively. In both cases, our computation is seen to capture the boundary layer with ease. To further understand error distribution we present maximum error for the previously mentioned two values of ε in Fig. 2.6c and 2.6d respectively. As could be expected, a relatively higher error was recorded in the regions with high gradients.

2.5.7 Test problem 7

Following Mohanty and Dey [104] and recent works of Lin and Reutskiy [97] as well as Reutskiy and Lin [124] we further implement the newly developed scheme for the following 3D nonlinear elliptic PDE with mixed derivatives

$$-a_1\left(\phi_{xx}+\phi_{yy}+\phi_{zz}\right)+d_1\phi_{xy}+d_2\phi_{yz}+d_3\phi_{zx}-b\phi\left(\phi_x+\phi_y+\phi_z\right)=f(x,y,z) \quad (2.42)$$

where

$$a_1(x,y,z) = -(1+e^{x+y+z}),$$
$$d_1(x,y,z) = 1+\sin(x)\cos(y)\cos(z),$$
$$d_2(x,y,z) = 1+\cos(x)\sin(y)\cos(z),$$
$$d_3(x,y,z) = 1+\cos(x)\cos(y)\sin(z).$$

The exact solution defined inside and on a unit cube

$$\phi(x,y,z) = e^x\cos(y)\sin(z) \quad (2.43)$$

provides for source function $f(x,y,z)$. This solution doesn't possess sharp features and hence does not necessarily attract nonuniform grids. Nevertheless, to validate our nonuniform code we employ grids generated using equation (2.27) with $\alpha_x = \alpha_y = \alpha_z = 1.01$.

In order to discretize equation (2.42) with $b = 1,\ 10,\ 10^2,\ 10^3$, Mohanty and Dey [104] implemented a fourth-order single-cell FD scheme on uniform cubic grids of sizes $9\times9\times9$, $17\times17\times17$ and $33\times33\times33$. On the other hand, Lin and Reutskiy [97]

Table 2.8: Test problem 7: Comparison of maximum error and order of convergence of different methods.

Grid size	[97]	[124]	[104]		Present scheme	
	Max error	Max error	Max error	order	Max error	order
			$b = 1$			
$9 \times 9 \times 9$			1.17e-6		4.08e-8	
$17 \times 17 \times 17$			7.31e-8	4.00	3.07e-9	3.73
$33 \times 33 \times 33$			2.97e-9	4.62	1.94e-10	3.98
30050 NFP	—	—				
			$b = 10$			
$9 \times 9 \times 9$			1.96e-6		7.94e-8	
$17 \times 17 \times 17$			1.24e-7	3.98	6.56e-9	3.60
$33 \times 33 \times 33$			7.62e-9	4.02	5.23e-10	3.65
30050 NFP	1.67e-6	7.02e-7				
			$b = 10^2$			
$9 \times 9 \times 9$			7.55e-5		2.27e-7	
$17 \times 17 \times 17$			4.83e-6	3.97	1.85e-8	3.62
$33 \times 33 \times 33$			3.01e-7	4.00	1.56e-9	3.57
30050 NFP	1.87e-6	6.52e-6				
			$b = 10^3$			
$9 \times 9 \times 9$			7.78e-4		3.17e-7	
$17 \times 17 \times 17$			6.39e-5	3.61	2.49e-8	3.67
$33 \times 33 \times 33$			4.41e-6	3.86	2.06e-9	3.60
30050 NFP	1.35e-6	8.47e-7				
			$b = 10^4$			
$9 \times 9 \times 9$			—		5.58e-7	
$17 \times 17 \times 17$			—	—	3.14e-8	4.15
$33 \times 33 \times 33$			—	—	2.17e-9	3.85
30050 NFP	1.46e-6	1.05e-6				

employed a cubic B-spline semi-analytical algorithm whereas Reutskiy and Lin [124] worked with a redial basis function (RBF) based method for solving this problem. Numerical solutions calculated with $b = 10$, $b = 10^2$, $b = 10^3$ and $b = 10^4$ with a number of free parameters (NFP) of 30050, 60100 and 120200 can be found in both of these works. These numbers roughly correspond to number of mesh points

associated with grids $33 \times 33 \times 33$, $41 \times 41 \times 41$ and $51 \times 51 \times 51$ respectively. This inspired us to run numerical simulations for $b = 1$, 10, 10^2, 10^3 and 10^4 on nonuniform grids of sizes same as those of [104]. In Table 2.8, we have presented the numerically approximated maximum error and order of convergence. The computed data from Table 2.8 vividly illustrates the accuracy and effectiveness of the present formulation. The proposed scheme not only projects the least erroneous solution but also reports a higher order of convergence in all cases.

2.5.8 Test problem 8

Finally, in order to highlight the versatility of the new 19-point scheme, we compare it to a fully compact 27-point scheme. We consider linear PDE with the second-order cross-derivative terms in the unit cube $[0, 1]^3$ represented as in [3]

$$10\left(\phi_{xx} + \phi_{yy} + \phi_{zz}\right) + \phi_{xy} + 2\phi_{yz} + 3\phi_{zx} - 13\phi_x + 11\phi_y + 10\phi_z - 7\phi = f(x, y, z). \quad (2.44)$$

The Dirichlet boundary conditions and the forcing function f are chosen so as to conform to the analytical solution

$$\phi(x, y, z) = \exp(x + y + z). \quad (2.45)$$

We use uniform mesh to solve this problem and compare our results to those of

Table 2.9: Test problem 8: Maximum error of ϕ for different scheme on grids of different sizes and order of convergence.

Grid size	[3]		Present scheme		$\phi(0.5, 0.5, 0.5)$
	Max error	order	Max error	order	
5×5	2.53e-4		7.34e-6		4.4816589355
9×9	1.64e-5	3.95	6.35e-7	3.53	4.4816870689
17×17	1.04e-6	3.98	4.52e-8	3.81	4.4816889762

Ananthakrishnaiah *et al.* [3] in Table 2.9. This table further includes numerically estimated values of ϕ at $(0.5, 0.5, 0.5)$ along with the maximum error and order of convergence. Although [3] converges with a faster rate, it is found that our scheme has better accuracy for all the grids considered. Nevertheless, it appears that the newly developed formulation consistently comes close to a convergence of order four.

The table shows that even for the coarse $5 \times 5 \times 5$ grid, the numerical solution at the center of the cube estimated up to the tenth decimal place remains accurate.

2.6 Conclusion

This chapter pertains to a compact FD scheme for generalized 3D steady CDE. The newly proposed scheme developed on nonuniform grid does not employ any transformation between the physical plane and the computational plane. The scheme is seen to be quite efficient in capturing boundary or transitional layers present in the solution domain. By employing a flexible discretization strategy our scheme is seen to be quite adaptable to the singularities in the domain. In 3D, the scheme uses at most nineteen neighboring nodal points and is computationally efficient for stiffer choices of parameters. To the best of the authors' knowledge, this is the first attempt to compactly approximate 3D generalized CDE on nonuniform grids. Further extension of the discretization strategy in the presence of nonlinear as well as linear reaction terms is found to be rather straightforward. The scheme exhibit close to fourth-order of numerical convergence. A comprehensive comparison is carried out with some of the best-known discretization procedures of the CDE available in the literature. These comparisons indeed reveal the superior accuracy virtues of the present scheme especially in the presence of boundary layers.